Electronic Supplementary Information

Boosting Reverse Water-Gas Shift Reaction Activity of Pt Nanoparticles through Light Doping of W

Daiya Kobayashi,*[a,b] Hirokazu Kobayashi,*[b] Kohei Kusada,[b,c] Tomokazu Yamamoto,[d,e] Takaaki Toriyama,[e] Syo Matsumura,[d,e] Shogo Kawaguchi,[f] Yoshiki Kubota,[g] Masaaki Haneda,[h,i] Susan Meñez Aspera,[j] Hiroshi Nakanishi,[j] Shigebumi Arai[a] and Hiroshi Kitagawa*[b]

[a]*Nippon Soda Co. Ltd., Chiba Research Center, 12-54 Goi-minamikaigan, Ichihara, Chiba 290-0045, Japan.*

[b]*Division of Chemistry, Graduate School of Science, Kyoto University, Kitashirakawa-Oiwakecho, Sakyo-ku, Kyoto 606-8502, Japan.*

[c]*The Hakubi Center for Advanced Research, Kyoto University, Kitashirakawa Oiwakecho, Sakyo-ku, Kyoto 606-8502, Japan.*

[d]*Department of Applied Quantum Physics and Nuclear Engineering, Graduate School of Engineering, Kyushu University, Motooka 744, Nishi-ku, Fukuoka 819-0395, Japan.*

[e]*The Ultramicroscopy Research Center, Kyushu University, Motooka 744, Nishi-ku, Fukuoka 819-0395, Japan.*

[f]*Japan Synchrotron Radiation Research Institute (JASRI), SPring-8, 1-1-1 Kouto, Sayo-cho, Sayo-gun, Hyogo 679-5198, Japan.*

[g]*Department of Physical Science, Graduate School of Science, Osaka Prefecture University, Sakai, Osaka 599-8531, Japan.*

[h]*Advanced Ceramics Research Center, Nagoya Institute of Technology, 10-6-29 Asahigaoka, Tajimi, Gifu, 507-0071, Japan.*

[i]*Frontier Research Institute for Materials Science, Nagoya Institute of Technology, Gokiso-cho, Showa-ku, Nagoya, 465-8555, Japan.*

[j]*National Institute of Technology, Akashi College, 679-3 Nishioka, Uozumi, Akashi, Hyogo 674-8501, Japan.*

Table of Contents

Experimental Procedures

Preparation of γ-Al_2O_3-loaded PtW NP and Pt NP catalysts: A mixture of hexane (25 mL) and oleylamine (1.0 mL) suspension containing of PtW NPs (16.7 mg, for 10 mg Pt) was sonicated for 30 min in a 110-mL vial. Subsequently, 30 mL of 2-propanol solution containing AKP-G15 γ-Al_2O_3 (183.3 mg) support was added to the PtW NP suspension. The suspension was sonicated for another 60 min and centrifuged. The resulting gray powder was washed several times with a mixture of ethanol and hexane. Finally, the gray powder was collected by centrifugation using acetone. The same procedure was also used for Pt NPs/C.

Preparation of γ-Al_2O_3-loaded Pt NPs + WO_3 catalysts: A mixture of hexane (25 mL) and oleylamine (1.0 mL) suspension containing Pt NPs (12.2 mg, for 10 mg Pt) and WO_3 clusters (10.4 mg) was sonicated for 60 min in a 110-mL vial. Subsequently, 30 mL of 2- propanol solution containing AKP-G15 γ-Al_2O_3 (187.8 mg) support was added to the Pt NP and WO_3 cluster suspensions. The suspension was sonicated for another 60 min and centrifuged. The resulting gray powder was washed several times with a mixture of ethanol and hexane. Finally, the gray powder was collected by centrifugation using acetone.

Transmission electron microscopy (TEM) observation: The TEM images were captured using a Hitachi HT7700 operated at 100 kV accelerating voltage.

X-ray diffraction (XRD) measurements: The crystal structure and size of Pt NPs/Al_2O_3 and PtW NPs/ Al_2O_3 were investigated by powder XRD analysis using a Rigaku MiniFlex600 (Cu *K*α radiation).

Inductivity coupled plasma optical emission spectrometer (ICP-OES) measurements: Pt and W ratios in PtW NPs and Pt NPs were investigated using a Thermo Fisher Scientific iCAP 7600 Duo.

Scanning Transmission electron microscopy(STEM) observation and energy dispersive X-ray spectroscopy (EDX) analysis: High-resolution STEM images and STEM-EDX mapping images were captured using a JEOL JEM-ARM200F STEM instrument operated at an accelerating voltage of 200 kV.

In situ synchrotron XRD measurements: Pt NPs and PtW NPs were used without a support. Crystal sizes were investigated by capillary synchrotron XRD analysis under 1-bar H_2 conditions at each temperature with the BL02B2 beamline, SPring-8. The XRD patterns of the samples sealed in a glass capillary were measured in situ at a wavelength of 0.6298 Å.

Procedure for Le Bail fitting with Rigaku MiniFlex600: Le Bail fitting was performed using the TOPAS software (version 3.0; Bruker AXS). The FP function was used for profile refinement. Fitting was performed after subtracting the peaks attributed to alumina. The obtained parameters were fixed for the refinement of Pt NPs/Al_2O_3 and PtW NPs/ Al_2O_3.

Procedure for Le Bail fitting with SPring-8: Le Bail fitting was performed using the TOPAS software (version 3.0; Bruker AXS). Pearson VII function was used for profile refinement. The contribution of the experimental setup to the peak shape was obtained after performing Le Bail fitting of the CeO_2 standard. The obtained parameters were fixed for the refinement of Pt NPs/Al_2O_3 and PtW NPs/ Al_2O_3.

X-ray fluorescence (XRF) measurements: Pt, W, and Al_2O_3 atomic ratios in Pt NPs/Al_2O_3, PtW NPs/ Al_2O_3, and Pt NPs + WO_3 clusters/Al_2O_3 were investigated using a Rigaku ZSX Primus IV.

FT-IR measurements: FT-IR spectra of adsorbed CO_2 and CO as probe molecules were obtained to evaluate the CO_2 and CO adsorption states. The samples (10 mg) were placed in a diffuse reflection cell. After increasing the temperature from room temperature to 500 °C (20 °C/min) under a flow of 5% H_2/N_2 (30 mL/min), the samples were maintained at 500 °C for 1 h. They were subsequently purged with He and cooled to 200 °C. IR measurements in a CO_2 atmosphere were performed at 200 °C for 15 min under a flow of 0.5% CO_2/He.

In addition, IR measurements in a CO atmosphere were performed at 300 °C for 15 min under a flow of 0.5% CO/He after the same pre-treatment as that used for CO_2 adsorption. IR spectra were recorded using a Nicolet Nexus 670 FT-IR spectrometer, accumulating 64 scans at a resolution of 2 cm^{-1}.

Catalytic activity measurements: The catalytic tests were performed using fixed-bed flow reactor (BEL-REA, Microtrac BEL Corp., Japan), connected to a gas chromatograph (Shimadzu GC-2014). Aluminum-supported catalysts containing 3.65 mg of Pt were placed between pieces of glass wool in the middle of the reactor tube. The catalytic test was performed using a gas mixture of 10 sccm CO_2, 30 sccm H_2, and He 20 sccm at 100, 200, 300, 400, and 450 °C, and 6.7 bar. For the pre-treatment of the catalysts, the gas mixture was allowed to flow for 2 h at each temperature before performing the catalytic tests. The products were analyzed by flame ionization gas chromatography. The CO_2 conversion rate was calculated according to the following equation:

CO_2 conversion (%) = (([CO_2]inlet – [CO_2]out) / [CO_2]inlet) × 100,

where [CO_2]inlet and [CO_2]out represent the inlet and outlet CO_2 concentrations, respectively.

Investigation of the temperature dependence of the crystal size: Each sample was exposed to a mixture of 10 sccm CO_2, 30 sccm H_2, and 20 sccm He at 7.2 bar at 200, 300, or 400 °C, respectively. XRD measurements were then performed, and the average crystal size at each temperature was determined from the Le Bail fitting results.

Repeated tests of CO_2 hydrogenation reaction: Repeated tests were performed using a fixed-bed flow reactor (BEL-REA, Microtrac BEL Corp., Japan), connected to a gas chromatograph (Shimadzu GC-2014). Aluminum-supported catalysts containing 3.65 mg of Pt were placed between pieces of glass wool in the middle of the reactor tube. Repeated tests were performed at 400 °C using a gas mixture of 10 sccm CO_2, 30 sccm H_2, and 20 sccm He at 7.2 bar. During catalyst pre-treatment, the gas mixture was allowed to flow for 2 h at 200, 300, and 400 °C before performing the catalytic tests. In addition, the gas mixture was allowed to flow at 400 °C for 2 h before each of the five replicate tests. The products were analyzed by flame ionization gas chromatography. The CO_2 conversion rate was calculated as described above.

Computational details and d-band center calculation: DFT calculations were carried out using the Vienna *ab initio* simulation package (VASP).[1-4] The exchange–correlation term was described using generalized gradient approximation (GGA) based on the Perdew–Burke–Ernzerhof (PBE) functional.[5-8] The interaction between ions and electrons was analyzed using the projector augmented wave (PAW) method. [9,10] Plane-wave basis sets were employed with an energy cut-off of 600 eV. Slab models were used with 3×3 fcc (111) surfaces, six atomic layers, and a 30-Å-thick vacuum space. For the PtW alloy, 93 Pt atoms and 3 W atoms are present in the supercell (Figure S5 (a)). Electric dipole correction was used to cut the dipole interactions between the repeated image slabs. The surface Brillouin zone integrations for slab model calculations were performed on a grid of 5×5×1 k-points using a Methfessel–Paxton smearing[11] of σ = 0.2 eV. A conjugate-gradient algorithm [12] was used to relax the ions in the upper five atomic layers to their ground states. The positions of the bottom layer atoms are fixed with the bulk nearest atomic distance, 2.811 Å of $Pt_{31}W$. Figure S5 (b) shows the d-band centers, which are the average energies of the unoccupied and occupied states in the d-levels relative to the Fermi level.

Results and Discussion

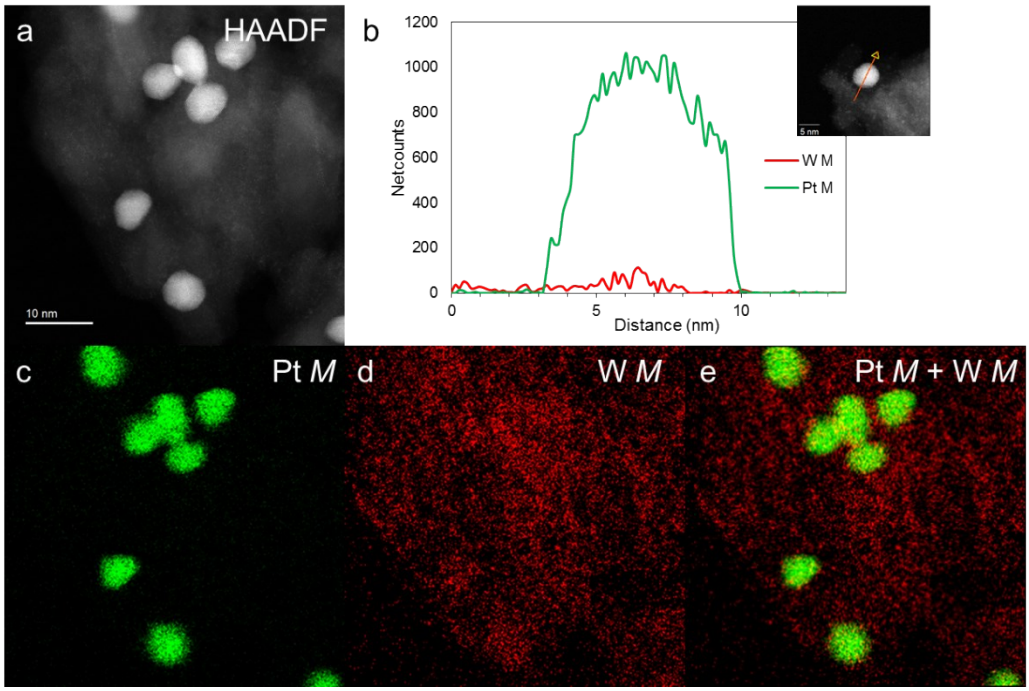

Figure S1. (a) HAADF-STEM image of PtW NPs/Al_2O_3; (b) compositional line profiles of Pt (green) and W (red) recorded along the arrow shown in the STEM image; (c) Pt-*M* and (d) W-*M* STEM-EDX maps; and (e) reconstructed overlay image of the maps shown in panels c and d (green, Pt; red, W).

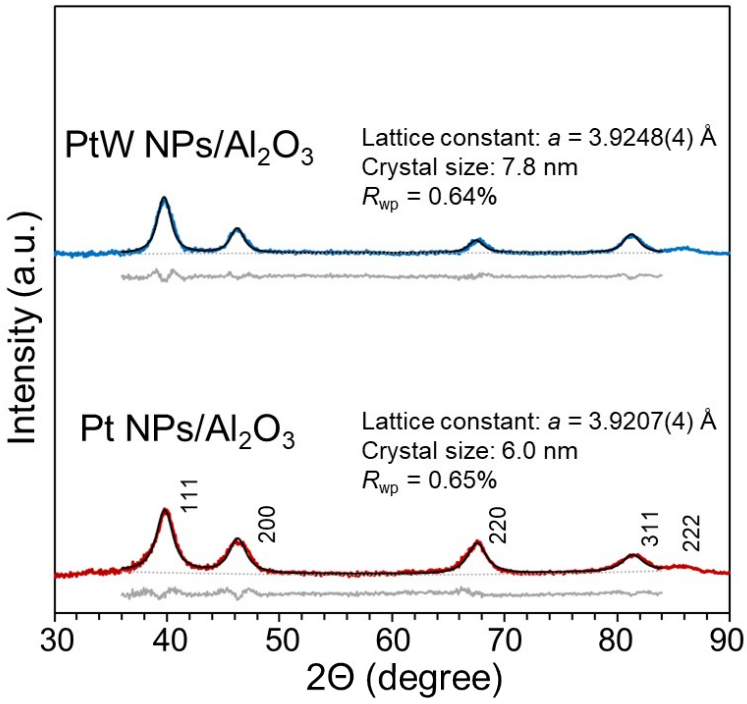

Figure S2. XRD patterns of Pt NPs/Al_2O_3 (red line) and PtW NPs/Al_2O_3 (blue line). These patterns have fitting curves (black line), difference profiles (gray line), and background (dotted line).

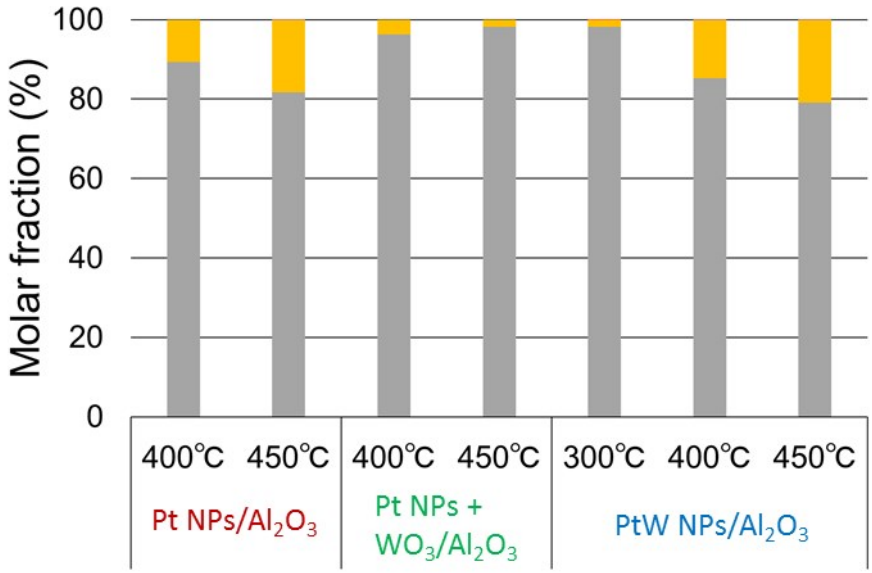

Figure S3. Product selectivity in RWGS reaction (gray: CO and yellow: CH_4).

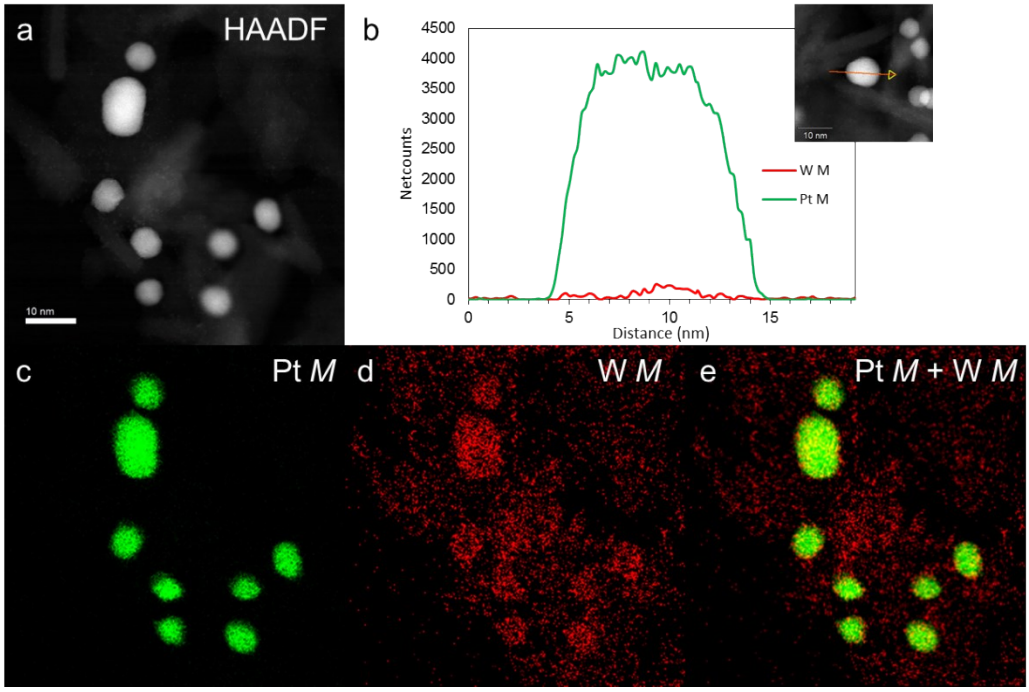

Figure S4. (a) HAADF-STEM image of PtW NPs/Al_2O_3 after reaction, (b) compositional line profiles of Pt (green) and W (red) recorded along the arrow shown in the STEM image, (c) Pt-*M* and (d) W-*M* STEM-EDX maps, and (e) reconstructed overlay image of the maps shown in panels c and d (green, Pt; red, W).

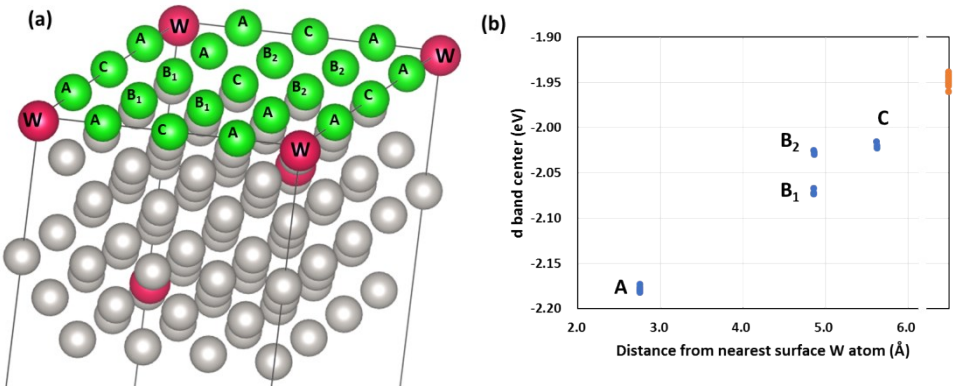

Figure S5. Slab model for PtW surface (a) and the corresponding d-band center values of each surface atom (b). Red balls indicate W atoms. Green (A, B1, B2, and C) and gray balls indicate surface and subsurface Pt atoms, visualized using the VESTA software.[13] Blue (A, B1, B2, and C) and orange dots in (b) are the d-band centers of corresponding surface Pt atoms on $Pt_{31}W$ alloy in (a) and those of surface atoms on pure Pt crystal, respectively.

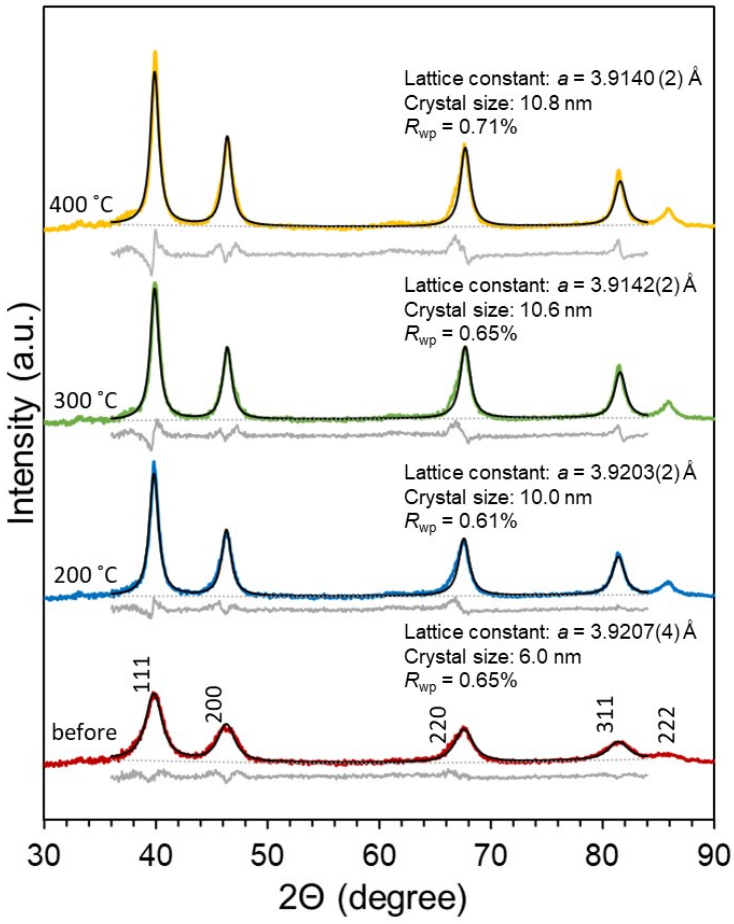

Figure S6. XRD patterns of Pt/Al_2O_3 NPs before (red line) and the after RWGS reaction at 200 °C (blue line), 300 °C (green line), and 400 °C (yellow line). These patterns have fitting curves (black line), difference profiles (gray line) and background (dotted line).

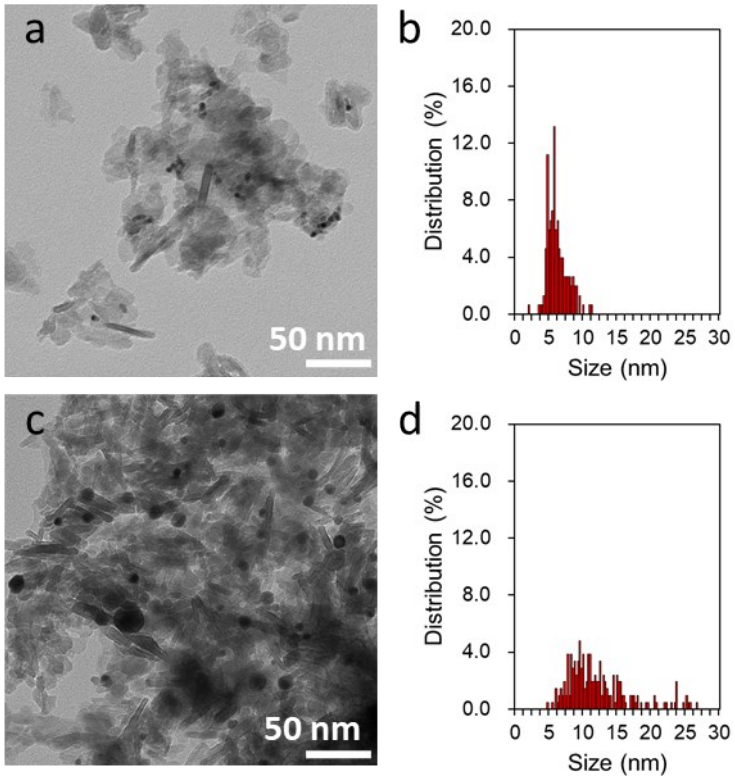

Figure S7. TEM images and size distributions for Pt NPs/Al_2O_3 (a, b) before and (c, d) after the RWGS reaction.

Before and after the reaction, the average particle size increased 2.0 times from 6.0 nm to 12.0 nm.

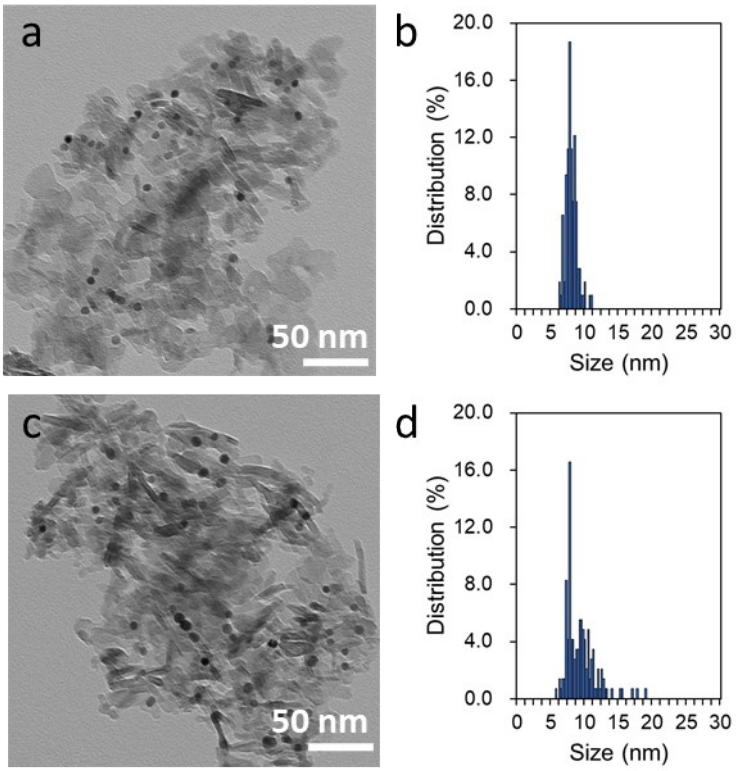

Figure S8. TEM images and size distributions for PtW NPs/Al_2O_3 (a, b) before and (c, d) after the RWGS reaction.

Before and after the reaction, the average particle size increased 1.2 times from 7.8 nm to 9.2 nm. It was confirmed that the increase in the particle size of PtW NPs/Al_2O_3 was suppressed compared to that of Pt NPs/Al_2O_3.

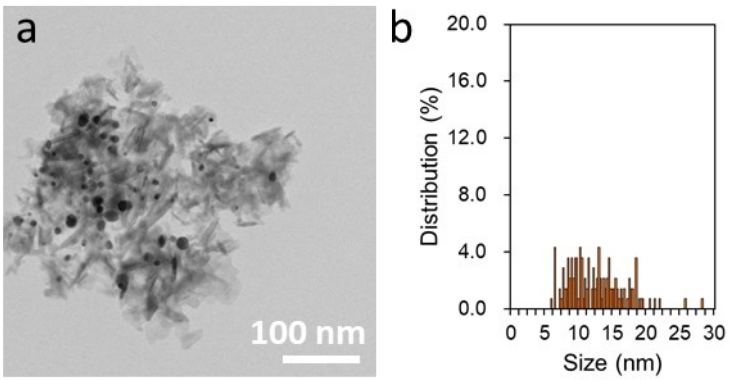

Figure S9. (a) TEM image and (b) size distribution for Pt NPs + WO_3/Al_2O_3 with an average particle size of 12.4 nm after the RWGS reaction.

Before and after the reaction, the average particle size of Pt NPs + WO_3/Al_2O_3 also became twice that of Pt NPs/Al_2O_3.

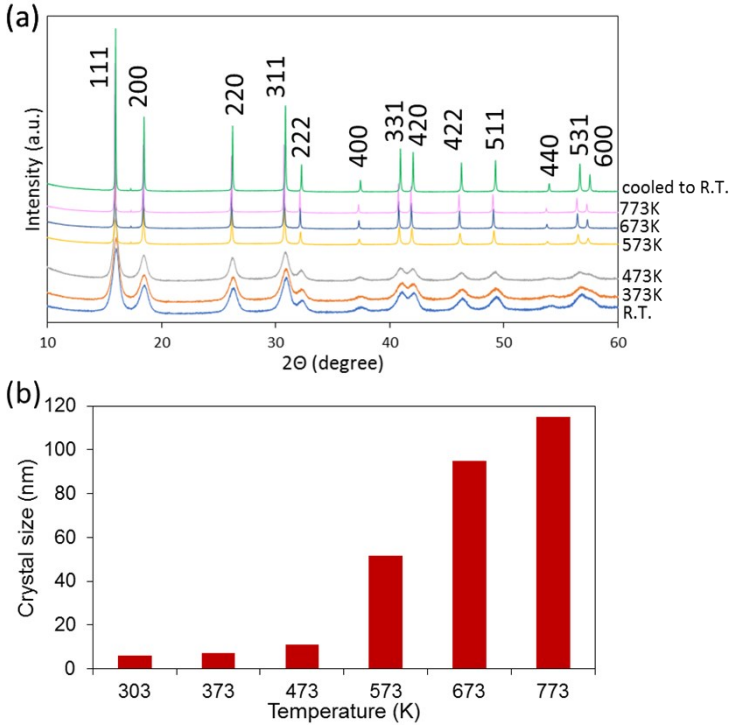

Figure S10. In situ synchrotron XRD measurements under hydrogen gas at 303 (R.T.)–773 K. XRD patterns at different temperatures for Pt NPs (a). Crystal sizes estimated by fitting the diffraction patterns at different temperatures for Pt NPs (b).

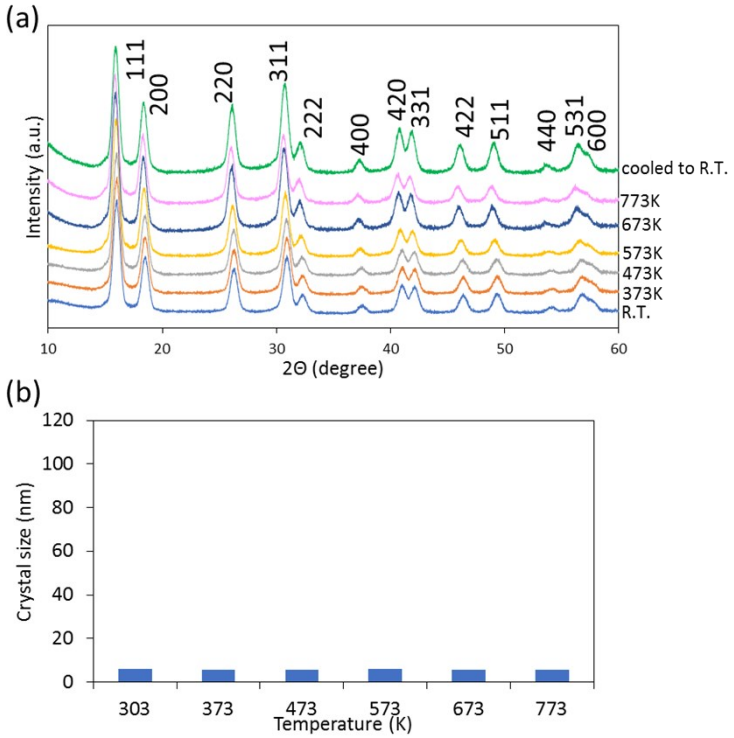

Figure S11. In situ synchrotron XRD measurements under hydrogen gas at 303 (R.T.)–773 K. XRD patterns at different temperatures for PtW NPs (a). Crystal sizes estimated by a fitting of the diffraction patterns at different temperatures for PtW NPs (b).

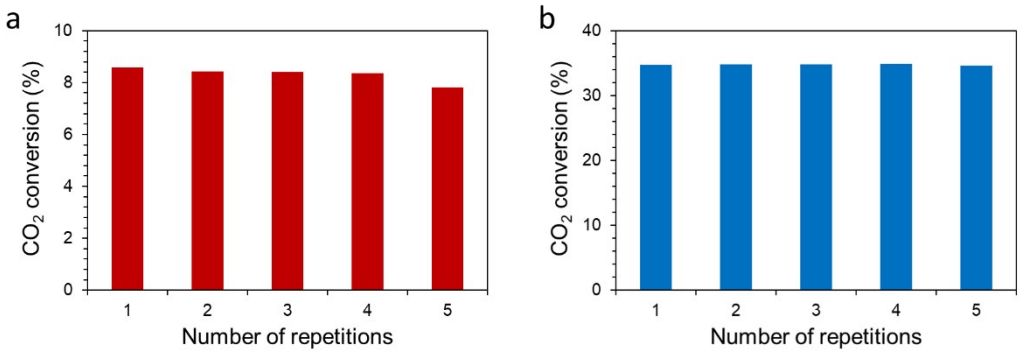

Figure S12. Five repeated RWGS reactions at 400 °C. CO_2 conversion using (a) Pt NPs/Al_2O_3 and (b) PtW NPs/Al_2O_3.

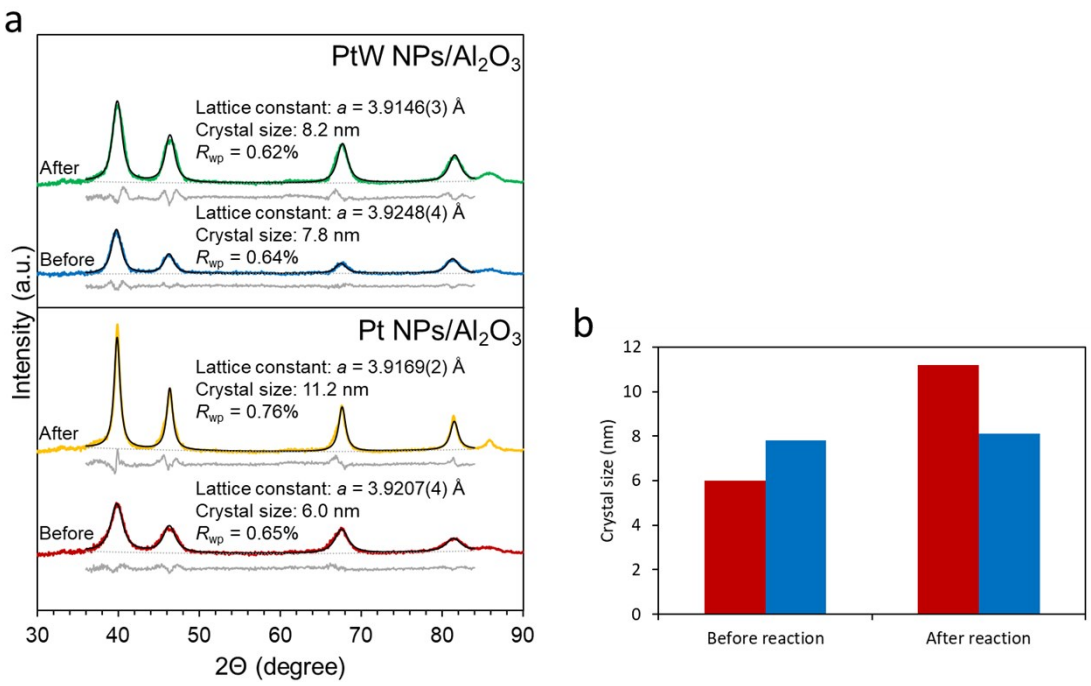

Figure S13. (a) XRD patterns of Pt NPs /Al_2O_3 before (red line) and after (yellow line) the repeated tests, and PtW NPs/Al_2O_3 before (blue line) and after the repeated tests (green line). These patterns have fitting curves (black line), difference profiles (gray line), and background (dotted line). (b) Calculated crystal size before and after five repeated tests using Pt NPs/Al_2O_3 (red) and PtW NPs/Al_2O_3 (blue).

Table S1. Pt, W, and Al_2O_3 ratio in PtW NPs/Al_2O_3 determined by XRF measurements.

Element	Weight Percentage
Pt	5.2
W	1.5
Al_2O_3	93.3

Table S2. Pt and W ratios of PtW NPs/Al_2O_3 determined by EDX measurements.

Area	Element	Atomic Percent
1	Pt	92.6
	W	7.4
2	Pt	94.9
	W	5.1
3	Pt	94.5
	W	5.5
4	Pt	97.5
	W	2.5
5	Pt	95.5
	W	4.5
6	Pt	92.4
	W	7.6
7	Pt	87.9
	W	12.1
8	Pt	91.9
	W	8.1

Table S3. Pt and Al_2O_3 ratios in Pt NPs/Al_2O_3 determined by XRF measurements.

Element	Weight Percentage
Pt	5.0
Al_2O_3	95.0

Table S4. Pt, W, and Al_2O_3 proportions in Pt NPs + WO_3/Al_2O_3 determined by XRF measurements.

Element	Weight Percentage
Pt	4.4
W	1.6
Al_2O_3	94.0

References

[1] G. Kresse and J. Furthmuller, *Phys. Rev. B: Condens. Matter Mater. Phys*., 1996, **54**, 11169.

[2] G. Kresse and J. Furthmuller, *Comput. Mater. Sci*., 1996, **6**, 15.

[3] G. Kresse and J. Hafner, *Phys. Rev. B: Condens. Matter Mater. Phys*., 1993, **47**, 558.

[4] G. Kresse and J. Hafner, *Phys. Rev. B: Condens. Matter Mater. Phys*., 1994, **49**, 14251.

[5] J. Perdew, K. Burke and M. Ernzerhof, *Phys. Rev. Lett*., 1996, ***77***, 3865.

[6] J. Perdew and K. Burke, *Phys. Rev. B: Condens. Matter Mater. Phys*., 1996, **54**, 16533.

[7] A. Becke, *Phys. Rev. A: At., Mol., Opt. Phys*., 1988, **38**, 3098.

[8] C. Lee, W. Yang and R. Parr, *Phys. Rev. B: Condens. Matter Mater. Phys*., 1988, **37**, 785.

[9] P. Blochl, *Phys. Rev. B: Condens. Matter Mater. Phys*.,1999, **59**, 17953.

[10] G. Kresse and J. Joubert, *Phys. Rev. B: Condens. Matter Mater. Phys*., 1999, **59**, 1758.

[11] M. Methfessel and A. Paxton, *Phys. Rev. B*, 1989, **470**, 3616.

[12] I. Stich, R. Car, M. Parrinello and S. Baroni, *Phys. Rev. B: Condens. Matter Mater. Phys*., 1989, **39**, 4997.

[13] K. Momma and F. Izumi, *J. Appl. Crystallogr*., 2011, **44**, 1.